AE International – Asia

Atmospheric Environment 38 (2004) 1869–1878

ATMOSPHERIC ENVIRONMENT

www.elsevier.com/locate/atmosenv

A drought-based predictor of recent haze events in western Indonesia

Robert D. Field[a,*], Yonghe Wang[a], Orbita Roswintiarti[b], Guswanto[c]

[a] Natural Resources Canada, Canadian Forest Service, Northern Forestry Centre, 5320-122 Street, Edmonton, Alta., Canada T6H 3S5
[b] Indonesian National Institute of Aeronautics and Space, Jl. Pemuda Persil No. 1, Jakarta Timur 13220, Indonesia
[c] Indonesian Bureau of Meteorology and Geophysics, Jl. Angkasa I/2 Kemayoran, Jakarta Pusat 10720, Indonesia

Received 8 August 2003; accepted 12 January 2004

Abstract

Indonesia's fire and haze problem is reviewed, and a model quantifying the relationship between drought and haze from biomass burning in western Indonesia is presented. Visibility observations from weather stations in Sumatra and Kalimantan were used as a haze indicator. The Drought Code component of the Canadian Forest Fire Weather Index System was used as a drought indicator. Using meteorological data from 1994 to 1998, we obtained regional haze and drought signals for western Indonesia. Nonlinear regression analysis was performed between the two signals to obtain a model of haze potential based on the Drought Code. Using the curvature properties of the nonlinear model, we estimated that severe haze is likely above a threshold Drought Code of 388.2. Using this threshold value, we propose four levels of drought that can be used operationally as an early warning tool in managing Indonesia's serious haze problem.

Keywords: Air quality; Forest fires; Peat; El Niño; Bootstrap

1. Introduction

Haze is a serious consequence of land and forest fires in Indonesia and is arguably among Indonesia's worst environmental problems. Fires in Indonesia occur primarily during the dry-season months of June–September and are more frequent and severe during El Niño years due to a pronounced rainfall deficit (Chandra et al., 1998; Wooster et al., 1998; Kita et al., 2000; Siegert and Hoffmann, 2000; Roswintiarti and Raman, 2003). During the drought and haze disasters of 1997 and 1998, direct and indirect costs were estimated at between US$ 8.7 and 9.2 billion (ADB and BAPPENAS, 1999). These costs included negative local impacts on transportation, agriculture, timber and nontimber forest resources, and, in particular, human health (Nichol, 1998; Heil and Goldammer, 2001; Siegert et al., 2001; Kunii et al., 2002; Sastry, 2002). Significant local impacts were also felt during the 1994 haze event (Nichol, 1997; Salafsky, 1997), though to a lesser degree than in 1997 and 1998. The global significance of emissions from Indonesian forest fires is also well established (Herman et al., 1997; Levine, 1999; Thompson et al., 2001; Ji and Stocker, 2002; Page et al., 2002; Cochrane, 2003).

Siegert et al. (2001) estimated the area burned by fires in the province of East Kalimantan from August 1997 until July 1998 at 5 million ha. Siegert and Hoffmann (2000) also examined the East Kalimantan fires of 1998, qualitatively describing the association between increasing drought and fire occurrence. The established link between drought and haze in East Kalimantan indicated that a similar relationship might exist for all of western Indonesia. Furthermore, we wanted to determine if this relationship could be quantified, specifically, whether

*Corresponding author. Fax: +1-780-435-7359.
E-mail address: rfield@nrcan.gc.ca (R.D. Field).

1352-2310/$ - see front matter
doi:10.1016/j.atmosenv.2004.01.011

occurrence of haze was related to a given level of drought.

Fires in peatlands are the major factor contributing to smoke production in Indonesia (Nichol, 1997, 1998; Levine, 1999; Heil and Goldammer, 2001; Ikegami et al., 2001; Page et al., 2002; Cochrane, 2003). We adopted the Drought Code (DC) component of the Canadian Forest Fire Weather Index (FWI) system, part of the Canadian Forest Fire Danger Rating System (CFFDRS), described by Lee et al. (2002), as our drought indicator, because it estimates the moisture content of deep (10–20 cm), compact organic layers such as peat, and is used as an indicator of long-term drying and the potential for deep, smoldering fires (Van Wagner, 1987; McAlpine, 1990). The DC can be described as a moisture accounting system for deep organic and heavy surface fuels; it increases during dry, hot days, and is lowered after rainfall. The DC has an unbounded scale, but for reference purposes, values typically reach a maximum of between 500 and 600 in the driest regions of Canada (McAlpine, 1990).

The practice of adopting an existing fire danger rating system for use in other regions is well established, with components of the CFFDRS having been used in Florida and Mexico (Lee et al., 2002), southern Europe (Xavier-Garcia et al., 1999) and New Zealand (Fogarty et al., 1998). There is an urgent need for the development of fire danger rating systems in Southeast Asia, and in Indonesia in particular (ASEAN, 2003). Given the severe impacts of the haze produced from peat fires, our intent here was to test the DC for operational use in assessing the potential for severe haze events.

2. Data and methods

2.1. Drought and visibility data

Meteorological data were obtained from the Global Surface Summary of the Day of the National climatic data centre (NCDC) (available at http://www.ncdc.noaa.gov); data were available for January 1994 to August 2000 at the time the data were acquired. This dataset was derived from operational synoptic meteorological data archived from the Global Telecommunications System, and underwent significant quality control at the NCDC in addition to that done at the Indonesian Bureau of Meteorology and Geophysics (BMG).

The DC is usually calculated on a daily basis using temperature at 1200 local standard time (LST), 24-h rainfall accumulated at 1200 LST and the previous day's DC value, for continuous and real-time drought monitoring (Lee et al., 2002). In this study, mean daily temperature was used in place of 1200 LST observations, which were not available in the NCDC data set. Twenty-four hour rainfall totalled at 0000 UTC (0700 or 0800 LST in Sumatra and Kalimantan) was used in place of rainfall totalled at 1200 LST, which was also not available. Rainfall data were missing for the period January to September 1999, and the analysis period was therefore restricted to the 5-year period from 1994 to 1998. Because of its cumulative nature, the FWI system requires continuous weather observations; missing temperature and rainfall values were estimated spatially using the inverse-distance-weighting scheme implemented in the Spatial Fire Management System (Lee et al., 2002; Englefield, 2000).

A limited number of stations were used for the analysis because of variability in data quality. Weather stations were selected on the basis of rainfall data completeness because of its governing influence on the DC. As in Manton et al. (2001), we used 80% daily data completeness as the minimum for a station to be included in the analysis. In all, eight of the 41 available stations over Sumatra and Kalimantan met this criterion, with a mean completeness of rainfall data across the eight stations of 87.9%. The World meteorological organization (WMO) identifiers and locations of the stations were: 960350 (3.57°, 98.68°), 961090 (0.47°, 101.45°), 961710 (−0.47°, 102.32°), 962210 (−2.90°, 104.70°), 966450 (−2.70°, 111.70°), 966550 (−1.00°, 114.00°), 966850 (−3.43°, 114.75°), 966330 (−1.27°, 116.90°). This level of data coverage was comparable to the study of Manton et al. (2001), which encompassed 91 stations, but over a much larger region, ranging from Myanmar to French Polynesia and extending as far south as New Zealand. The stations were all located in low-lying areas of Sumatra and Kalimantan (Fig. 1).

The NCDC dataset also included daily mean visibility, used to indicate haze. Visibility observations were also used by Heil and Goldammer (2001) to describe the decrease in air quality during the 1997 fires. In that study, decreased visibility was associated with increased concentration of particulate matter, as measured by total suspended particulate matter (TSP) and particulate matter with diameter $\leqslant 10\,\mu m$ (PM_{10}). Visibility was also used as a surrogate for particulate matter concentrations in an analysis by Schictel et al. (2001) of haze trends in the United States. Visibility was hence an appropriate proxy for air quality in our study, particularly given the serious health impacts of particulate matter emissions from biomass burning (Heil and Goldammer, 2001; Kunii et al., 2002).

Visibility observations, used primarily for aviation purposes, are recorded in kilometres of visible distance, measured using local landmarks as reference points (Schictel et al., 2001). To standardize the data for any analysis across multiple stations, visibility was expressed as a percentage of normal visibility. We selected 1995 as the reference year because of the absence of a severe haze event in Sumatra and Kalimantan in that year

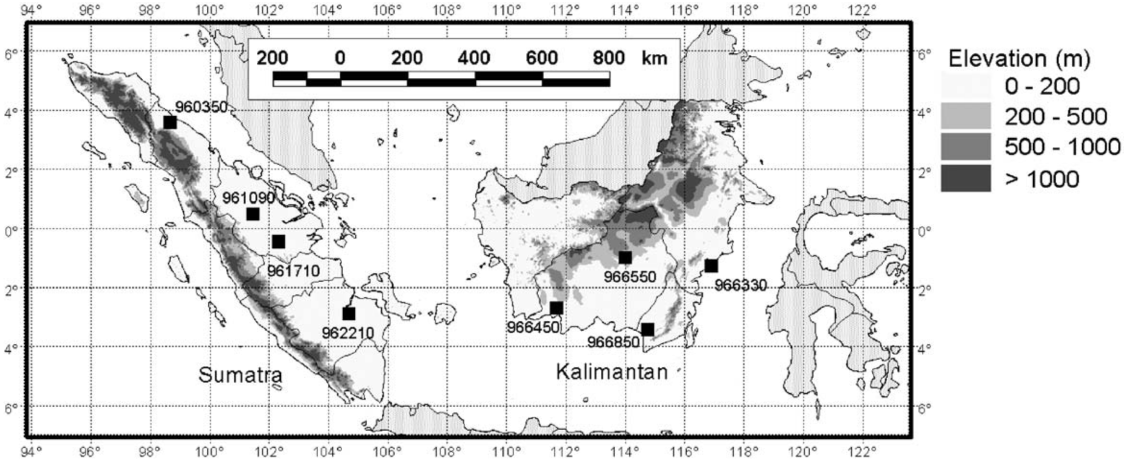

Fig. 1. Sumatra and Kalimantan elevation with analysis station locations.

(Fujiwara et al., 1999; Kita et al., 2000; Radojevic, 2003). Each station's visibility observations were expressed as a percentage of the mean 1995 visibility for that station, which normalized the data across differences in local observation standards and ambient visibility levels. Over the selected stations, mean 1995 visibility ranged from 6.8 to 9.2 km, with an average of 8.2 km.

Expressing individual station visibility as a percentage of its 1995 mean allowed us to obtain a daily visibility time series for the region. Daily visibility values from the eight analysis stations were averaged, similar to the spatial averaging of TOMS data by Kita et al. (2000) and Thompson et al. (2001). We obtained a regional DC signal by averaging across the eight stations, with station coverage assumed to be distributed evenly enough to warrant an unweighted mean. The result was a daily time series consisting of 1819 observations for both visibility and DC. For the regression analysis between the two time series, we did not perform any temporal smoothing, to allow the analysis to reflect how both variables would be available operationally and to preserve the full daily variability of both regional signals. Given the short length of the data record, we did not examine the underlying spatial dependence between individual weather stations.

We also considered a regional drought code anomaly (DCA) as a predictor variable. Drought and fire in Indonesia are frequently described as occurring during exceptionally dry El Niño years (e.g. Kita et al., 2000). Our expectation, therefore, was that an anomaly based predictor variable would distinguish rare events from normal dry seasons and perhaps offer an improvement in haze predictability by removing the seasonality of the raw DC signal. The DCA was calculated by subtracting the 5-year monthly DC mean from the daily DC signal. We then determined whether a significant relationship existed between visibility and either the DC or the DCA signal, collectively referred to as drought in the next sections.

The absence of severe haze events during non El Niño dry seasons (Kita et al., 2000; Bowen et al., 2001) suggested a threshold level of drought, below which haze events are unlikely and above which they are expected. The concept of a threshold drought level is also physically appropriate, because of the well-defined relationship between peat fuel moisture and ignition (Frandsen, 1997). Such threshold levels are of key operational importance for fire management, because they act as "triggers" in preventive fire management decision-making, particularly at a national scale during disaster-level conditions. The estimation of DC and DCA thresholds was therefore an integral aspect of our analysis.

2.2. Model development

We modeled the relationship between regional visibility and drought using nonlinear regression analysis. A linear model would not have been appropriate, as it would associate a linear increase in drought with a linear decrease in the visibility, which would not be the case under a threshold-driven system. The model used was the standard four-parameter logistic curve, in our case defined by the function

$$\mu\{\mathrm{VIS}|X\} = \mathrm{VIS}_{\mathrm{MAX}} + (\mathrm{VIS}_{\mathrm{MIN}} - \mathrm{VIS}_{\mathrm{MAX}}) \times \left[1 + \exp\left(\frac{X_{\mathrm{MID}} - X}{S}\right)\right]^{-1}, \quad (1)$$

where the independent variable X was either DC or DCA and $\mu\{\mathrm{VIS}|X\}$ was the mean visibility response for a given drought level X. The parameters estimated were maximum visibility, $\mathrm{VIS}_{\mathrm{MAX}}$; minimum visibility,

VIS_{MIN}; the mid point, X_{MID}; and the horizontal scale, S.

The shape of the parameterized function allowed for the definition of two threshold values. The first was the point at which the visibility began to decrease rapidly with increasing values of X, and the second was the point at which the curve began to flatten out with increasing X, tending toward its lower asymptote. These regions can also be thought of as intervals over which the function exhibits maximum curvature. The curvature $\kappa(X)$ of a function $f(X)$ is defined formally as

$$\kappa(X) = \frac{|f''(X)|}{[1 + (f'(X))^2]^{3/2}}. \tag{2}$$

We maximized the function $\kappa(X)$ to accurately obtain the two points of maximum curvature. The locations of these points are most closely associated with the X_{MID} and S that define the shape of the curve between the two asymptotes, VIS_{MAX} and VIS_{MIN}. Increasing values of X_{MID} will increase the value of X at which the point of maximum curvature is obtained, and increasing values of S will decrease the value of X at which the point of maximum curvature is obtained.

The first point of maximum curvature was the drought level at which visibility began to decrease rapidly, hence, was an appropriate level at which to trigger fire management activities. To evaluate whether the DC-based or the DCA-based model provided the best threshold, we determined which one had the most constrained threshold ranges and which provided the best separation between below-threshold and above-threshold visibility values. The second point of maximum curvature was not used, as it corresponded to a saturation level of atmospheric pollution and therefore cannot contribute to early warning.

2.3. Statistical treatment

The bootstrap method (Efron and Tibshirani, 1993) was used to determine the uncertainty of the threshold. This method is a nonparametric and data-based simulation technique for making statistical inferences. It entails repeated sampling of the data and parameter estimation, to obtain a distribution of model parameter estimates, from which statistical inference is then made. As Efron and Tibshirani (1993) describe, the typical number of bootstrap samples ranges from 50 to 200 for standard error estimation. We therefore took 200 random samples from our original data (with replacement), each sample composed of 1819 DC- or DCA-visibility pairs.

Visual examination showed that the data were highly skewed toward low DC or DCA and high visibility values, because of the infrequency of severe drought and haze conditions. Such a skewed distribution may pose a problem in model fitting, owing to the risk that some bootstrapped samples could be dominated by the low DC or DCA and high visibility values, which would bias the parameter estimates. As a result, we stratified the data into the following four subsets on the basis of DC value: $DC<200$, $DC\geqslant200$ and $DC<400$, $DC\geqslant400$ and $DC<600$, and $DC\geqslant600$. Five hundred random with-replacement observations were taken from each of the four strata, with parameter estimates taken over the 2000 pooled observations. This process was repeated 200 times to form our 200 bootstrap samples as Efron and Tibshirani (1993) recommended.

We fitted Eq. (1) to each of the 200 samples, and from the fitted model obtained 200 sets of parameter estimates. For each of the 200 bootstrap-fitted models, the threshold values were computed by numerical maximization of curvature $\kappa(X)$, as defined in Eq. (2). As a result, we had an empirical distribution of 200 threshold values for both the DC-based or DCA-based models. To obtain 95% confidence intervals for the parameters and threshold values, we calculated the 2.5th and 97.5th percentiles from each of their empirical distributions.

2.4. Secondary class boundaries

In keeping with the concept of early warning, we also defined levels of mobilization corresponding to increasing drought levels. These drought levels indicated the extent to which the current DC or DCA is approaching its threshold value. We used the number of days without rainfall required to reach the threshold level, and defined four classes (LOW, MODERATE, HIGH, EXTREME) separated by three class boundary levels. The class boundaries between HIGH and EXTREME, MODERATE and HIGH, and LOW and MODERATE classes were defined by the DC or DCA after which 5, 15 or 30 days without rain respectively would result in the threshold value. We calculated these secondary boundary levels after estimating the threshold drought values. When calculating these secondary levels, we used a constant temperature of 27.1°C as input to the DC, which was the mean temperature observed across the 8 stations during the analysis period. For this fixed temperature, the DC increases by 8.2 points per day without rain.

3. Results and discussion

3.1. Regional visibility and drought signals

Regional visibility (Fig. 2a) showed two strong haze signals during the dry seasons of the 1994 and 1997 El Niño years, and a weaker haze signal in early 1998. During non haze periods, regional visibility was characterized by day-to-day variability between the 80% and 120% levels (relative to 1995).

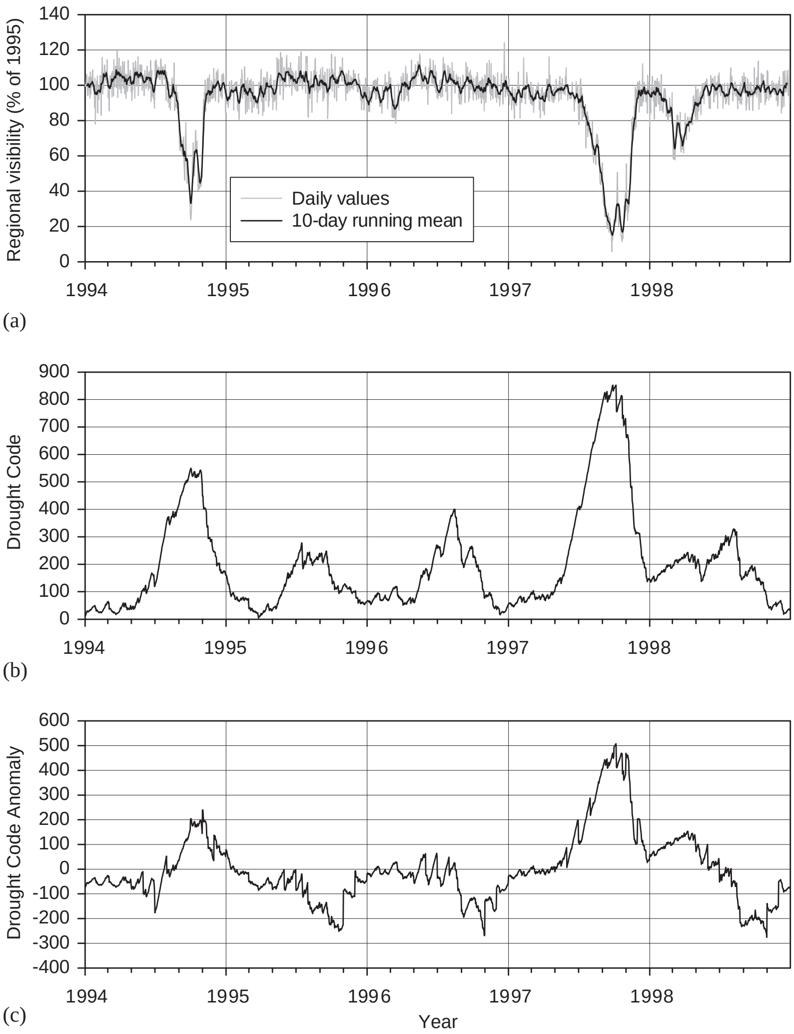

Fig. 2. (a) Daily regional visibility along with its 10-day running mean, (b) daily DC and (c) daily DCA across western Indonesia, 1994–1998. Labelled tick marks on horizontal axis are for 1 January of each year.

The visibility threshold of 80% defined the timing of the three haze events. During the 1994 haze event, visibility dropped below 80% on 1 September, and reached its minimum value of 33.1% on 1 October; the haze event ended on 4 November. During this 65-day period, the average visibility was 55.9%. The duration of the 1994 haze event as defined by regional visibility was consistent with air quality data observed in Singapore (Nichol, 1997). The 1997 haze event started on 23 July, a minimum visibility value of 15.1% was reached on 26 September, and the haze event ended on 21 November. The average visibility during this 121-day event was 42.8%. The 1997 event therefore lasted nearly twice as long as the 1994 event and was more severe over its duration.

The haze event in early 1998 was less severe than those in 1994 and 1997. It started on 28 February, minimum visibility of 64% was reached on 6 March, and the event ended on 19 April. Over the course of this 51-day haze event, the average visibility was 73.7%. The visibility signal over 1997 and 1998 corresponds closely to the TOMS Aerosol Index (AI) signal over Sumatra and Kalimantan (Thompson et al., 2001). In that study, the 1997 event was indicated as a persistent upward spike in the TOMS AI signal above the 0.5 level, and the 1998 haze event was seen as a smaller signal, with both spikes corresponding to increased detection of aerosol over the region. The different severities of the three events also correspond to their differing spatial extents (Radojevic, 2003).

The regional DC (Fig. 2b) showed a regular pattern of annual seasonality, corresponding to the tropical wet and dry seasons. As for visibility, the most apparent interannual difference was between the dry seasons of El Niño years and non El Niño years. Under El Niño dry-season conditions, the regional DC reached maximum values of 549 on 2 October in 1994 and 852 on 6 October in 1997. This was considerably higher than the maximum values of 277 on 16 July in 1995, 401 on 13 August in 1996, and 329 on 7 August in 1998.

The regional DCA (Fig. 2c) was similar to the regional DC, with a more apparent distinction between El Niño and non El Niño conditions. The peaks in regional DCA during the El Niño periods occurred on the same days as the peaks in the regional DC. The DCA maximum values of 205 and 507 units above normal occurred, respectively, during 1994 and 1997. During the non El Niño dry seasons of 1995, 1996 and 1998, the peaks in the DC disappeared in the DCA signal, owing to below-average dry-season DC values. The DCA signal also showed that there were unseasonably high DC values during the first four months of 1998. The DC signal alone did not show this, as it was obscured by the regular dry-season peaks from non El Niño years.

In comparing the visibility with the two drought signals, the most striking aspect was the absence of severe haze periods during the dry-season months of June to September in 1995, 1996 and 1998. Despite "normal" dry-season increases in the regional DC during these years, visibility values remained between 80% and 120% of normal during the dry-season months. This was consistent with the TOMS signals (Kita et al., 2000), and further confirms the existence of a threshold value for the DC and the DCA. Visual comparison of the two plots (Fig. 2) suggested a rough threshold of 400 for the DC and 50 for the DCA, corresponding to the peaks in the signals in 1996 during which no haze event occurred. The 50-day haze period in early 1998 was exceptional in that it occurred under regional DC values lower than those seen during the peaks of the 1995 and 1996 dry seasons. However, a higher DCA was associated with the weaker 1998 haze signal.

3.2. Model fitting and threshold estimation

Under both models, the VIS_{MAX} parameter was the best constrained, whereas the VIS_{MIN}, DC_{MID}, and S parameters exhibited wider ranges across the bootstrapped estimates (Table 1).

The models resulting from both sets of mean parameter estimates are shown in Fig. 3a and b, along with the observed data. In each plot, the curve was obtained by applying the parameter values listed in Table 1 to Eq. (1). The distribution of the 200 bootstrap-estimated threshold values for both models are shown in Figs. 2c and 2d. Under the DC model, the mean r^2 between data and predicted values across all 200 bootstrap samples was 0.81, with a mean residual error of 7.6%. This model had a sharper region of maximum curvature (Fig. 3a), resulting from the relatively low S parameter estimates. The DC threshold had a mean value of 388.2, a standard deviation of 5.4% and 95% confidence interval of (377.0, 398.8).

The DCA model had a mean r^2 of 0.78, slightly lower than that of the DC model and a slightly higher mean residual error (7.9%). This model had a more gradual region of maximum curvature (Fig. 3b) owing to the comparatively higher S parameter estimates. The DCA threshold had a mean value of 126.2, a standard deviation of 26.5% and 95% confidence interval of (76.2, 188.3), more than five times as wide as the threshold confidence interval for the DC model.

In comparing the goodness of fit of the two models, the most notable outliers were the 1998 haze event observations in the DC model. This event appears in Fig. 3a as a group of low-visibility observations in the 60–80% range just above a DC of 200. Though less severe than the 1994 and 1997 events, this event would still be considered serious from the perspective of the visibility anomaly adopted here and by local fire management agencies. These outlying observations are

Table 1
Summary statistics for bootstrapped parameter estimates from the DC and DCA models

	DC					DCA				
Parameter	Min.	Mean	Max.	SD	95%CI	Min.	Mean	Max.	SD	95%CI
VIS_{MAX}	99.9	101.8	103.8	0.8	(100.3, 103.4)	109.8	113.6	118.7	1.6	(110.7, 117.3)
VIS_{MIN}	3.2	19.6	28.7	4.3	(10.2, 26.9)	−114.7	−43.5	−13.1	17.0	(−88.5, −16.2)
X_{MID}	511.3	551.0	618.2	19.0	(517.4, 594.1)	309.7	401.5	563.6	43.4	(323.3, 510.7)
S	89.7	123.7	166.6	13.4	(98.9, 149.3)	169.2	209.1	264.0	16.0	(183.4, 246.2)
Threshold	370.1	388.2	406.0	5.4	(377.0, 398.8)	68.8	126.2	215.9	26.5	(76.2, 188.3)

SD = standard deviation, CI = confidence interval.

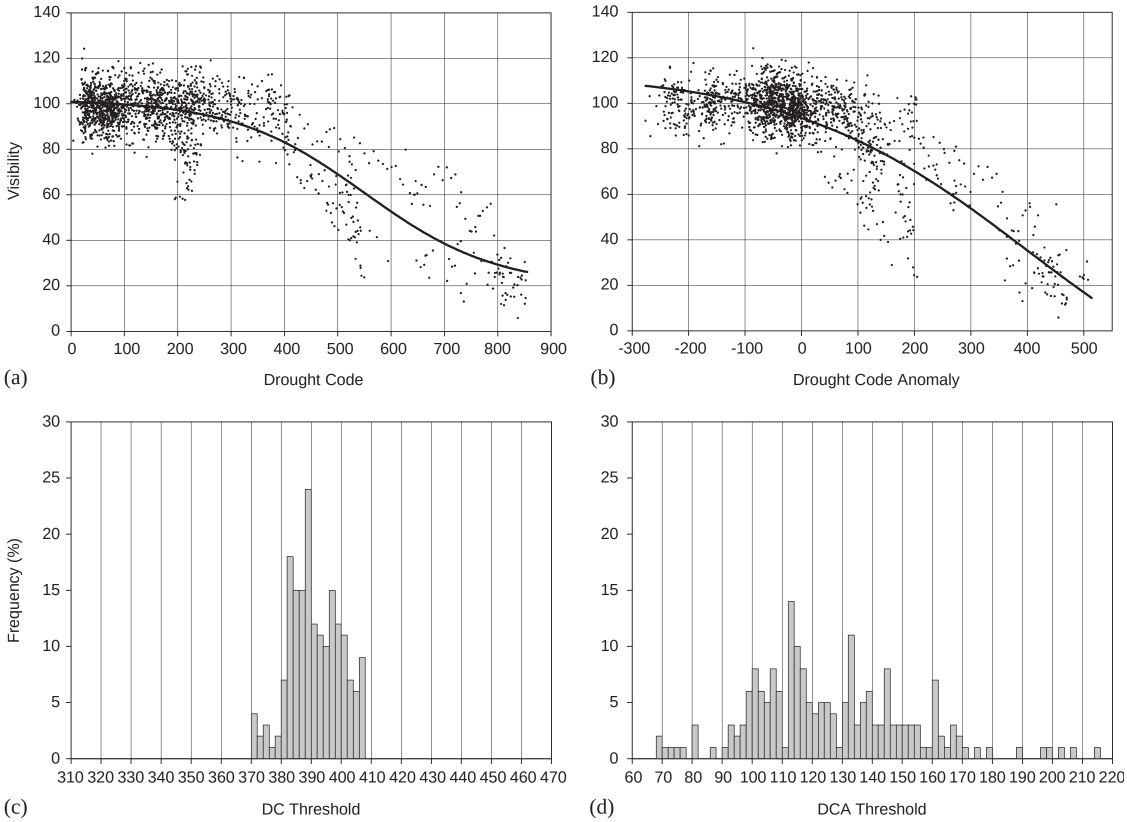

Fig. 3. Fitted models (a,b) and frequency distributions of bootstrapped threshold values (c,d) for the DC-based and DCA-based models. The models were based on the mean parameter estimates from 200 bootstrap iterations and also show the observed data.

less distinct under the DCA model, with the DCA signal (Fig. 2c) also showing unseasonably dry conditions for that time of year. However, because of the wide range in the DCA threshold distribution (Fig. 2d), the DC model was deemed more useful in determining a drought threshold level for operational application and hence was selected to define our mobilization levels.

3.3. Secondary DC class boundaries

Using a DC threshold value of 388.2, we calculated the mobilization class levels on the basis of the number of dry days required to reach that threshold level. The result, using the number of dry days defined in the methods, was that the HIGH–EXTREME boundary was defined by a DC of 346.9, the MODERATE–HIGH boundary by a DC of 264.4 and the LOW–MODERATE boundary by a DC of 140.7. The interpretation of the classes resulting from these boundary levels is as follows:

- EXTREME: The DC is approaching disaster-level drought conditions seen during 1994 and 1997. All fire management prevention and pre-preparedness measures should be mobilized.
- HIGH: The DC is approaching normal dry-season peak conditions. Weather forecasts and seasonal rainfall assessments should be monitored closely for signs of an extended dry-season.
- MODERATE: Normal mid dry-season conditions. Burning should be monitored as usual.
- LOW: Typical wet-season conditions. Severe haze periods unlikely.

Note that the number of dry days for the different levels was chosen somewhat arbitrarily. Given the simple relationship between the increase in DC and number of dry-days, the number of dry-days used to define the DC levels could be modified depending on the fire management context in which they were being implemented. Furthermore, specific fire management actions depend on the local burning practices, agricultural patterns and fuel types, and should be developed by local fire management experts.

In adopting the DC-based model to derive our mobilization classes, we wanted to better understand the anomalous 1998 event, which would not have been

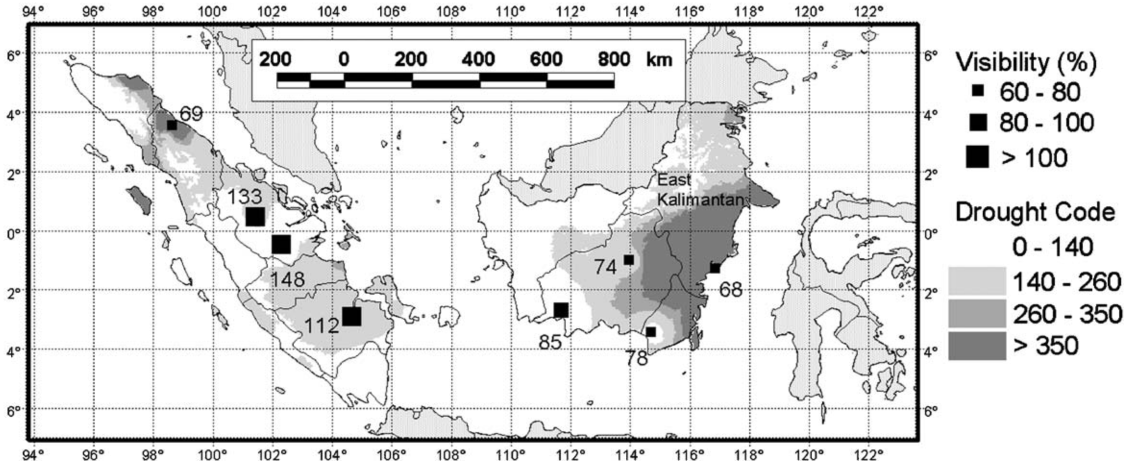

Fig. 4. DC and visibility across Sumatra and Kalimantan on 28 February, 1998, the approximate onset of the 1998 haze event. The gridded DC values in the map have been classified according to the estimated class boundaries after rounding to the nearest 10. Analysis stations are labelled and sized according to percent visibility.

predicted by the DC-based model nor caught by the DC mobilization levels described above if monitored by a single regional index. We therefore examined the spatial variation in drought conditions across western Indonesia that contributed to the regional DC signal, using the DC from all data input stations interpolated across Sumatra and Kalimantan on 28 February, 1998, the approximate onset date of the 1998 haze event (Fig. 4). The map also shows analysis station locations labelled and sized according to visibility level.

The anomalous 1998 event can be explained by the haze's greater spatial extent than the drought in Kalimantan. During the 1998 event, fires were restricted to the southeastern quarter of East Kalimantan (Siegert and Hoffmann, 2000), in roughly the EXTREME area seen in Fig. 4. The haze-affected area though, as indicated by the sub-80% visibility values, extends further west. Furthermore, examination of atmospheric conditions (not shown) displayed a southwestward flow from East to central Kalimantan, which allows us to conclude that the reduced visibility in central Kalimantan was the result of smoke transport and diffusion from fires in East Kalimantan. The outlying observations in 1998 can be therefore be explained by the local nature of the drought relative to the broader extent of the haze. While regional averaging was useful for analytical purposes, the case of East Kalimantan in 1998 underscores the importance of monitoring both regional and local drought conditions, and hence the utility of the spatial DC display seen in Fig. 4.

4. Conclusions

This study has provided a means by which to objectively monitor the potential for regional haze events in Sumatra and Kalimantan, based on the DC component of the Canadian FWI System. Analysis of regional visibility and DC over the period 1994–1998 showed that severe haze days occurred mostly above a DC threshold of 388.2 (95% confidence interval (379.5, 397.5)). Four DC classes were determined on the basis of the number of dry days required for the DC to reach this threshold value. The smaller haze episode in 1998 was not predicted by the regional DC threshold level, but was well explained by regional DCA values and by local DC levels in East Kalimantan.

From this analysis, we propose several recommendations for early-warning monitoring of severe haze episodes across Sumatra and Kalimantan. First, the use of visibility data as a monitoring tool should be adopted in Sumatra and Kalimantan, given the immediate availability of such data at synoptic-level stations. Visibility observations provide an excellent source of in situ data for use as a real-time proxy for air quality measurements, which are not yet available with nearly the same spatial or temporal coverage as the synoptic-level meteorological data (Nichol, 1998; Heil and Goldammer, 2001). In one sense, the visibility observations provide as much power to predict severe haze as the DC, as decreasing trends in visibility or increasing trends in DC both tend to be harbingers of subsequent severe haze.

In terms of early warning however, the clear advantage of the DC is that it can be predicted from simple trend analysis, weather forecasts and seasonal rainfall assessment, whereas the visibility cannot be predicted without first observing a decreasing trend in its signal. Thus the importance of monitoring both visibility and DC is paramount. To this end, BMG has begun monitoring and disseminating both visibility and DC data as part of its mandate as the early warning information provider for natural disasters in Indonesia. The cornerstone of this program is the daily production of fire danger maps for DC and other fire danger indices, similar to that in Fig. 3, using real-time data from BMG's synoptic station network.

We can also recommend areas for continued investigation in refining relationships between drought and haze occurrence. Because we included two El Niño events of different magnitudes in our analysis, our period of record was climatologically representative, but a longer record of daily meteorological data would be useful in validating the DC model. A denser network of weather stations would also be useful, in that it could contribute to a complete model of spatial dependence. Furthermore, any attribution of reduced visibility at "receptor" locations to drought and fire occurrence at "source" locations would necessarily require consideration of smoke transport effects, which was beyond the scope of this study. The coupling of fire danger models such as the DC model with atmospheric transport models as studied by Yonemura (2002), Koe et al. (2001, 2003) and Roswintiarti and Raman (2003) could also provide an early warning tool to capture the transport characteristics of smoke haze. Such operational systems would be particularly useful for early warning of events such as the 1998 haze episode, when localized drought and fire was responsible for transboundary haze. To this end, we are now conducting a retrospective transport simulation of the 1997 and 1998 haze events, examining the relationship between upstream drought conditions and downstream air quality.

Acknowledgements

The authors thank Bill de Groot, Caren Dymond and Steen Magnussen of the Canadian Forest Service and an anonymous reviewer for suggestions which greatly improved earlier versions of the manuscript. This work was carried out under the Southeast Asia Fire Danger Rating System Project, supported by the Canadian International Development Agency's Southeast Asia programme.

References

Asian Development Bank (ADB), National Development Planning Agency (BAPPENAS), 1999. Causes, extent, impact and costs of 1997/98 fires and drought. Final report, Annex 1 and 2. Planning for Fire Prevention and Drought Management Project. Asian Development Bank TA 2999-INO Fortech. Pusat Pengembangan Agribisnis, Margueles Pöyry, Jakarta, Indonesia.

Association of Southeast Asian Nations (ASEAN), 2003. ASEAN Agreement on Transboundary Haze Pollution. Available at http://www.haze-online.or.id, accessed March 2003.

Bowen, M.R., Bompard, J.M., Anderson, I.P., Guizol, P., Gouyon, A., 2001. Anthropogenic fires in Indonesia: a view from Sumatra. In: Eaton, P., Radojevic, M. (Eds.), Forest Fires and Regional Haze in Southeast Asia. Nova Science Publishers, Huntington, NY, pp. 41–66.

Chandra, S., Ziemke, J.R., Min, W., Read, W.G., 1998. Effects of 1997–1998 El Niño on tropospheric ozone and water vapor. Geophysical Research Letters 25, 3867–3870.

Cochrane, M.A., 2003. Fire science for rainforests. Nature 421, 913–919.

Efron, B., Tibshirani, R.J., 1993. An Introduction to the Bootstrap. Chapman & Hall, New York, NY, pp. 1–16.

Englefield, P., Lee, B.S., Suddaby, R., 2000. Spatial fire management system. In: ESRI User Conference Proceedings. Environmental Systems Research Institute, 380 New York street, Redlands, CA, Paper no. 489, 12p.

Fogarty, L.G., Pearce, H.G., Catchpole, W.R., Alexander, M.E., 1998. Adoption vs. adaptation: lessons from applying the Canadian forest fire danger rating system in New Zealand. In: Third International Conference on Forest Fire Research and 14th Conference on Fire and Forest Meteorology, Proceedings, Vol. 1, Luso, Portugal. University of Coimbra, Coimbra, Portugal, pp. 1011–1028.

Frandsen, W.H., 1997. Ignition probability of organic soils. Canadian Journal of Forest Research 25, 1471–1477.

Fujiwara, M., Kita, K., Kawakami, S., Ogawa, T., Komala, N., Saraspriya, S., Suripto, A., 1999. Tropospheric ozone enhancements during the Indonesian forest fire events in 1994 and 1997 as revealed by ground-based observations. Geophysical Research Letters 26, 2417–2420.

Heil, A., Goldammer, J.G., 2001. Smoke-haze pollution: a review of the 1997 episode in Southeast Asia. Regional Environmental Change 2, 24–37.

Herman, J.R., Bhartia, P.K., Torres, O., Hsu, C., Seftore, C., Celarier, E., 1997. Global distribution of UV-absorbing aerosols from Nimbus 7/Toms data. Journal of Geophysical Research 102, 16911–16922.

Ikegami, M., Okada, K., Zaizen, Y., Makino, Y., Jensen, J.B., Gras, J.L., Harjanto, H., 2001. Very high weight ratios of S/K in individual haze particles over Kalimantan during the 1997 Indonesian forest fires. Atmospheric Environment 35, 4237–4243.

Ji, Y., Stocker, E., 2002. Seasonal, intraseasonal, and interannual variability of global land fires and their effects on atmospheric aerosol distribution. Journal of Geophysical Research 107, 4697.

Kita, K., Fujiwara, M., Kawakami, S., 2000. Total ozone increases associated with forest fires over the Indonesian region and its relation to the El Niño-Southern Oscillation. Atmospheric Environment 34, 2681–2690.

Koe, L.C.C., Arellano, A.F., McGregor, J.L., 2001. Investigating the haze transport from 1997 biomass burning in Southeast Asia: its impact upon Singapore. Atmospheric Environment 35, 2723–2734.

Koe, L.C.C., Arellano, A.F., McGregor, J.L., 2003. Application of DARLAM to regional haze modeling. Pure and Applied Geophysics 160, 189–204.

Kunii, O., Kanagawa, S., Yajima, I., Hisamatsu, Y., Yamamura, S., Amagai, T., Ismail, T., 2002. The 1997 haze disaster in Indonesia: its air quality and health effects. Archives of Environmental Health 57, 16–22.

Lee, B.S., Alexander, M.E., Hawkes, B.C., Lynham, T.J., Stocks, B.J., Englefield, P., 2002. Information systems in support of wildland fire management decision making in Canada. Computers and Electronics in Agriculture 37, 185–198.

Levine, J.S., 1999. The 1997 fires in Kalimantan and Sumatra, Indonesia: gaseous and particulate emissions. Geophysical Research Letters 26, 815–818.

Manton, M.J., Della-Marta, P.M., Haylock, M.R., Hennessy, K.J., Nicholls, N., Chambers, L.E., Collins, D.A., Daw, G., Finet, A., Gunawan, D., Inape, K., Isobe, H., Kestin, T.S., Lefale, P., Leyu, C.H., Lwin, T., Maitrepierre, L., Ouprasitwong, N., Page, C.M., Pahalad, J., Plummer, N., Salinger, M.J., Suppiah, R., Tran, V.L., Trewin, B., Tibig, I., Yee, D., 2001. Trends in extreme daily rainfall and temperature in Southeast Asia and the South Pacific: 1961–1998. International Journal of Climatology 21, 269–284.

McAlpine, R.S., 1990. Seasonal trends in the drought code component of the Canadian forest fire weather index system. Information Report PI-X-97 E/F. Forestry Canada, Petawawa, Ont., 36p.

Nichol, J., 1997. Bioclimatic impacts of the 1994 smoke haze event in Southeast Asia. Atmospheric Environment 31, 1209–1219.

Nichol, J., 1998. Smoke haze in Southeast Asia: a predictable recurrence. Atmospheric Environment 32, 2715–2716.

Page, S.E., Siegert, F., Rieley, J.O., Beohm, H.D.V., Jaya, A., Limin, S., 2002. The amount of carbon released from peat and forest fires in Indonesia during 1997. Nature 420, 61–65.

Radojevic, M., 2003. Chemistry of forest fires and regional haze with emphasis on Southeast Asia. Pure and Applied Geophysics 160, 157–187.

Roswintiarti, O., Raman, S., 2003. Three-dimensional simulations of the mean air transport during the 1997 forest fires in Kalimantan, Indonesia using a mesoscale numerical model. Pure and Applied Geophysics 160, 429–438.

Salafsky, N., 1997. Drought in the rain forest, Part II: an update based on the 1994 ENSO event. Climatic Change 39, 601–603.

Sastry, N., 2002. Forest fires, air pollution, and mortality in Southeast Asia. Demography 39, 1–23.

Schictel, B.A., Husar, R.B., Falke, S.R., Wilson, W.E., 2001. Haze trends over the United States: 1980–1995. Atmospheric Environment 35, 5205–5210.

Siegert, F., Hoffmann, A.A., 2000. The 1998 forest fires in East Kalimantan (Indonesia): a quantitative evaluation using high resolution, multitemporal ERS-2 SAR images and NOAA-AVHRR hotspots data. Remote Sensing of the Environment 72, 64–77.

Siegert, F., Ruecker, G., Hinrichs, A., Hoffmann, A.A., 2001. Increased damage from fires in logged forest during droughts caused by El Niño. Nature 414, 437–440.

Thompson, A.M., Witte, J.C., Hudson, R.D., Guo, H., Herman, J.R., Fujiwara, M., 2001. Tropical tropospheric ozone and biomass burning. Nature 291, 2128–2132.

Van Wagner, C.E., 1987. Development and structure of the Canadian forest fire weather index system. Technical Report 35. Canadian Forestry Service, Ottawa, ON. 37p.

Wooster, M.J., Ceccato, P., Flasse, S.P., 1998. Indonesian fires observed using AVHRR. International Journal of Remote Sensing 19, 383–386.

Xavier-Garcia, D., Bovio, G., Ferreira, A., 1999. Comparative study of various methods of fire danger evaluation in Southern Europe. International Journal of Wildland Fire 9, 235–246.

Yonemura, S., Tsuruta, H., Maeda, T., Kawashima, S., Sudo, S., Hayashi, M., 2002. Tropospheric ozone variability over Singapore from August to December 1999. Atmospheric Environment 36, 2061–2070.